Continuous CO2 capture and reduction to CO by circulating transition-metal-free dual-function material in fluidized-bed reactors

Sasayama, Tomone; Ono, Yuya; Kosaka, Fumihiko; Liu, Yanyong; Chen, Shih-Yuan; Mochizuki, Takehisa; Matsuoka, Koichi; Urakawa, Atsushi; Kuramoto, Koji

DOI
10.1016/j.seppur.2024.128602

Publication date
2025

Document Version
Final published version

Published in
Separation and Purification Technology

Separation and Purification Technology 354 (2025) 128602

Contents lists available at ScienceDirect

Separation and Purification Technology

journal homepage: www.elsevier.com/locate/seppur

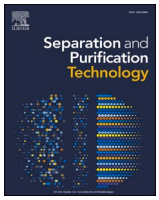

Continuous CO_2 capture and reduction to CO by circulating transition-metal-free dual-function material in fluidized-bed reactors

Tomone Sasayama [a], Yuya Ono [a], Fumihiko Kosaka [a,*], Yanyong Liu [a], Shih-Yuan Chen [a], Takehisa Mochizuki [a], Koichi Matsuoka [a], Atsushi Urakawa [b], Koji Kuramoto [a]

[a] National Institute of Advanced Industrial Science and Technology (AIST), 16-1 Onogawa, Tsukuba, Ibaraki 305-8569, Japan
[b] Catalysis Engineering, Department of Chemical Engineering, Delft University of Technology, Van der Maasweg 9, 2629 HZ Delft, the Netherlands

ARTICLE INFO

Editor: S. Yi

Keywords:
CO_2 capture
CO_2 utilization
Dual-function material
Circulating fluidized bed
Syngas

ABSTRACT

To mitigate global warming and achieve a sustainable society, innovative technologies for efficient CO_2 utilization are required. Integrated CO_2 capture and reduction (CCR) using dual-function materials (DFMs) is favorable owing to its potentially low energy consumption, capital investment, and processing costs. Although numerous studies have focused on catalytic science, continuous and steady-state CCR operations have not been sufficiently addressed from an engineering perspective. In this study, a circulating fluidized bed (CFB) system is investigated for continuous CCR to syngas (CO + H_2). In the CFB system, transition-metal-free DFM (Na/Al_2O_3) particles are circulated between two bubbling fluidized-bed reactors. The DFM captures CO_2 in one reactor (CO_2 capture reactor) and reduces the captured CO_2 to CO by the reaction with H_2 in the other reactor (H_2 reactor). The effluent gas concentrations from both reactors reach steady state and are maintained for over 8 h. For the product gas from the H_2 reactor, the CO_2 conversion and CO selectivity exceed 80 % and 99 %, respectively. However, the H_2 conversion is <20 %, indicating a potential challenge for the CFB system for integrated CCR. Furthermore, this study confirms that the H_2/CO ratio for syngas can be controlled by adjusting the experimental conditions (particularly, the H_2 flow rate). Consequently, the CFB system can be modified to facilitate the interaction between H_2 gas and the DFM particles.

1. Introduction

The Intergovernmental Panel on Climate Change (IPCC), in its sixth report, concluded that anthropogenic emissions of greenhouse gases (GHGs) have unequivocally caused global warming [1]. Global net emissions of the primary GHG, carbon dioxide, have continually increased and reached 59 $GtCO_2$-eq in 2019; more than 60 % of the CO_2 emissions were found to originate from fossil fuels and industry [2]. The development of innovative technologies for carbon dioxide capture, utilization, and storage (CCUS) is essential for controlling global warming and achieving a sustainable society. CCUS technologies generally require a series of operations such as CO_2 capture, desorption, purification, compression, and transportation before CO_2 utilization, including conversion or storage [3–8]. The utilization of CO_2 is preferable to its storage from the perspective of exploiting CO_2 as a carbon source to produce fuels and value-added chemicals.

Recently, various studies have been conducted to investigate the viability of integrated CO_2 capture and utilization (ICCU) or CO_2 capture and reduction (CCR), wherein CO_2 is captured by an absorbent and directly converted into the desired product without being desorbed. The advantage of CCR is that the operations between CO_2 capture and utilization are eliminated; thus, energy consumption and costs for capital investment and processing can be substantially reduced. Techniques for CO_2 capture using amine solutions have been combined with thermocatalytic [9–11] and electrocatalytic [12,13] CO_2 conversion. Although such gas–liquid absorption techniques are industrially established for CO_2 capture, amine solutions are typically unstable under heating conditions exceeding 100 °C and generate emissions of harmful thermal degradation products [14–16]. This limits the scope of CO_2 conversion reactions to those with sufficient reaction rates at extremely low temperatures. In contrast, the integration of CO_2 conversion with CO_2 capture using solid adsorbents is feasible at higher temperatures.

Abbreviations: CCR, CO_2 capture and reduction; CCUS, carbon dioxide capture, utilization and storage; CFB, circulating fluidized bed; DFM, dual-function material; DRM, dry reforming of methane; GHG, greenhouse gas; RWGS, reverse water gas shift.

* Corresponding author.
E-mail address: f.kosaka@aist.go.jp (F. Kosaka).

https://doi.org/10.1016/j.seppur.2024.128602
Received 6 December 2023; Received in revised form 19 June 2024; Accepted 26 June 2024
Available online 27 June 2024

Consequently, a greater variety of CO_2 conversion reactions, such as methanation, reverse water gas shift (RWGS), and dry reforming of methane (DRM), can be considered.

Dual-function materials (DFMs) which serve as both solid CO_2 sorbents and catalysts for CO_2 conversion have been proposed by pioneer research groups [17,18] and investigated by several researchers thus far. Alkali or alkaline earth metals including Na [19,20], K [21,22], and Ca [23,24] are typically employed as CO_2 sorbents in DFMs. Generally, Ca requires higher regeneration temperatures (>600 °C) to demonstrate its excellent capacity for CO_2 capture, whereas Na and K can be used at lower temperatures with less capacity [25]. Transition metals such as Ni [26–29], Ru [30,31], and Cu [21,22] are used in DFMs as catalysts to convert the captured CO_2 via the desired reaction. Ni is one of the most frequently used catalysts in DFMs because of its relatively low cost and versatile activity in catalyzing methanation, RWGS, and DRM, which are interchangeable depending on the reaction temperature [32,33]. We have previously reported CCR to CH_4 using Ni-based DFMs promoted with Na, K, and Ca [26]. Among the studied DFMs, Na/Ni/Al_2O_3 showed the highest CO_2 conversion exceeding 96 % and CH_4 selectivity exceeding 93 % at 450 °C and 0.1 MPa. By pressurizing from 0.1 to 0.9 MPa, the CH_4 production capacity was enhanced from 111 to 160 mmol/g with a model CO_2 source (400 ppm) to imitate direct air capture. Recently, we have further demonstrated that even transition-metal-free DFMs have remarkable activity against CCR to CO [20]. Na/Al_2O_3 exhibited excellent performance to achieve a CO_2 conversion exceeding 90 % and CO selectivity exceeding 95 % at 450–500 °C and 0.1 MPa. In addition, it showed the potential to produce syngas-like mixture with an H_2/CO molar ratio of 2–3 from atmospheric-level CO_2 (400 ppm). The absence of transition metals could be advantageous in terms of low material cost and environment-friendliness.

Owing to the early stages of technological development, most studies have primarily focused on catalytic science by developing novel DFMs. However, the engineering aspects of CCR have not been sufficiently emphasized. Studies on DFMs generally involve a fixed-bed reactor and intermittent alternating operations for CO_2 capture and reduction. Although material development is crucial, the development of novel CCR processes that enable continuous and steady-state operations is essential for industrialization. Continuous operations for CCR to CH_4 [34] and CO [35] have been demonstrated at the lab scale using two isothermal fixed-bed reactors packed with DFMs in parallel. This method enables an apparent steady-state capture and conversion by alternating the feed gases to each reactor. Another approach, namely, a circulating fluidized bed (CFB) system, was employed in our previous study for CCR to CH_4 [36] using approximately 1 kg of the Na/Ni/Al_2O_3 DFM. In the CFB system, DFM particles were continuously circulated between two fluidized-bed reactors instead of exchanging the feed gases. The advantage of this CFB system is that the temperature in each reactor can be controlled separately, and an actual steady state in terms of gas feed, effluent flow, and concentration, can be achieved.

In this study, the concept of continuous CCR to syngas (CO + H_2) is demonstrated by combining our knowledge of transition-metal-free Na/Al_2O_3 DFM [20] and the CFB system [36]. The obtained results are compared with previous results for CCR to CH_4 using a Na/Ni/Al_2O_3 DFM to determine the bottleneck that reduces the overall efficiency. Accordingly, the effects of the operating conditions are investigated to elucidate the characteristics of the CFB system and to maximize its performance for continuous CCR.

2. Materials and methods

2.1. Preparation and characterization of DFM

γ-Al_2O_3 (Neobead MSC#300, Mizusawa Industrial Chemicals, Ltd.) was used as a support for the DFM, and Na_2CO_3 (guaranteed reagent, Fujifilm Wako Pure Chemical Corp.) was used as the precursor. The transition-metal-free Na/Al_2O_3 DFM was prepared by the wet impregnation of an aqueous solution of Na_2CO_3 on γ-Al_2O_3. The impregnated samples were dried at 110 °C for 12 h and subsequently calcined in air at 550 °C for 4 h. The alkali-metal loading was set to 16 wt % in the carbonate form. The textural properties and crystalline structures of the prepared DFM was characterized by N_2 adsorption–desorption and powder X-ray diffraction (XRD) analyses, similar to our previously reported process [20]. In addition, the minimum fluidization velocity of the sample was experimentally determined from the relationship between the pressure drop in the DFM bed and the gas velocity, as described in the Supplementary Material.

2.2. Continuous CCR to CO in the CFB system

Fig. 1 shows a schematic of the CFB setup. Approximately 600 g of the prepared Na/Al_2O_3 DFM was loaded into the CFB system and continuously circulated in two bubbling fluidized-bed reactors, i.e., the CO_2 capture and H_2 reactors. The CO_2 capture reactor was maintained at 200–500 °C with external heating, and 2 vol% CO_2/N_2 (flow rate = 8 L/min) was supplied to the bottom of the reactor. The Na sites in the DFM selectively captured CO_2 in this reactor. The flow rate of the CO_2-containing gas was sufficiently high to fluidize the DFM particles in the CO_2 capture reactor and to entrain the DFM particles from the reactor to a cyclone through the riser. The entrained DFM particles and the CO_2-lean gas entered the cyclone, where they were separated. The vented CO_2-lean gas was analyzed using a dual-channel micro gas chromatograph (GC) equipped with thermal conductivity detectors (Agilent 490, Agilent Technologies, Inc.) after water vapor was condensed.

Subsequently, the DFM particles were accumulated in the upper loop seal, preventing the undesired mixing of gases between the two reactors. As N_2 was supplied to the loop seal at a relatively low flow rate of approximately 0.15 L/min, the overflowing DFM particles were continuously entrained to the H_2 reactor. The H_2 reactor was maintained at 500–700 °C with an electric heater, and H_2 was supplied to the bottom of the reactor at a flow rate of 0.4–2.0 L/min. In this reactor, the DFM

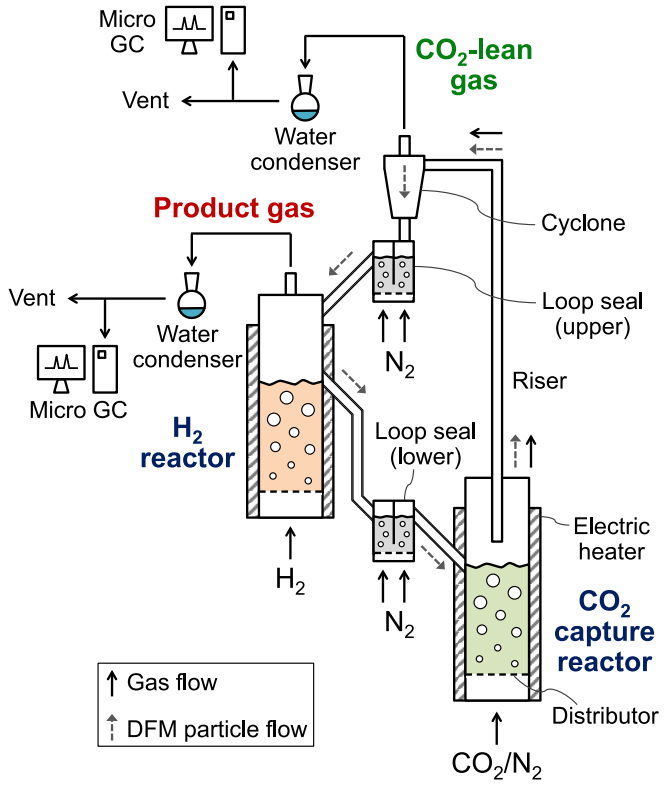

Fig. 1. Schematic of the circulating fluidized bed (CFB) system with Na/Al_2O_3 dual-function material (DFM).

particles were regenerated by releasing the captured carbon, primarily as CO. Subsequently, the DFM particles returned to the CO_2 capture reactor through the lower loop seal. The product gas was vented from the top of the H_2 reactor and analyzed using a micro-GC after water vapor was condensed.

For quantitative analysis, the data obtained from the CO_2 capture reactor was used to calculate the CO_2 capture efficiency (η_{CO_2}) as follows:

$$\eta_{CO_2} = \left(1 - \frac{C_{CO_2-R_{CO_2.out}}}{C_{CO_2-R_{CO_2.in}}}\right) \times 100 \quad (1)$$

where $C_{CO_2-R_{CO_2.in}}$ and $C_{CO_2-R_{CO_2.out}}$ represent the CO_2 concentrations in the feed gas stream and the CO_2-lean gas exiting the CO_2 capture reactor, respectively. Using the data obtained from the H_2 reactor, the CO_2 conversion (X_{CO_2}), selectivity for CO or CH_4 (S_{CO}, S_{CH_4}), and H_2 conversion (X_{H_2}) were calculated as follows:

$$X_{CO_2} = \left(1 - \frac{C_{CO_2-R_{H_2.out}}}{C_{CO_2-R_{H_2.out}} + C_{CO-R_{H_2.out}} + C_{CH_4-R_{H_2.out}}}\right) \times 100 \quad (2)$$

$$S_{CO} = \frac{C_{CO-R_{H_2.out}}}{C_{CO-R_{H_2.out}} + C_{CH_4-R_{H_2.out}}} \times 100 \quad (3)$$

$$S_{CH_4} = \frac{C_{CH_4-R_{H_2.out}}}{C_{CO-R_{H_2.out}} + C_{CH_4-R_{H_2.out}}} \times 100 = 100 - S_{CO} \quad (4)$$

$$X_{H_2} = \left(1 - \frac{C_{H_2-R_{H_2.out}}}{C_{H_2-R_{H_2.out}} + C_{CO-R_{H_2.out}} + 4C_{CH_4-R_{H_2.out}}}\right) \times 100 \quad (5)$$

where $C_{i-R_{H_2.out}}$ represents the concentration of i (i = CO_2, CO, CH_4, or H_2) in the product gas exiting the H_2 reactor.

3. Results and discussion

3.1. Characterization of DFM

The characteristics of the prepared DFM are briefly described in this section. Further details are provided in the Supplementary Material. N_2 adsorption–desorption analysis revealed that Na impregnation did not markedly damage the porous structure of the alumina support (Table S1). In the XRD analysis, the distinct diffraction peaks of γ-Al_2O_3 and extremely small peaks of Na_2CO_3 were detected (Fig. S1), indicating that the Na sites were well dispersed on the alumina support. As presented in Fig. S2 and Table S2, the relationship between the pressure drop in the DFM bed and the gas velocity was used to determine the minimum fluidization velocities, which were found to be 1.2, 1.1, and 0.99 cm/s at 300, 400, and 500 °C, respectively. Considering the inner diameters of the reactors (approximately 3.8 cm), the minimum fluidization velocities were converted to 0.82, 0.76, and 0.68 L/min at 300, 400, and 500 °C, respectively.

3.2. Demonstration of continuous CCR to CO in the CFB system

The experimental results of continuous CCR in the CFB system using the transition-metal-free Na/Al_2O_3 DFM are presented in Fig. 2. Here, the CO_2 capture reactor was maintained at 400 °C, the temperature and H_2 feed flow rate in the H_2 reactor were set to 500 °C and 0.8 L/min, respectively. Fig. 2(a) shows the concentration profile of the CO_2-lean gas exiting the CO_2 capture reactor. Immediately after the CO_2-containing gas was supplied to the CO_2 capture reactor, the CO_2 concentration gradually increased and remained constant for over 8 h. The dashed line in the figure indicates the feed CO_2 concentration. This indicates that approximately half of the fed CO_2 was continuously captured in the DFM. One or more carbonation reactions listed below

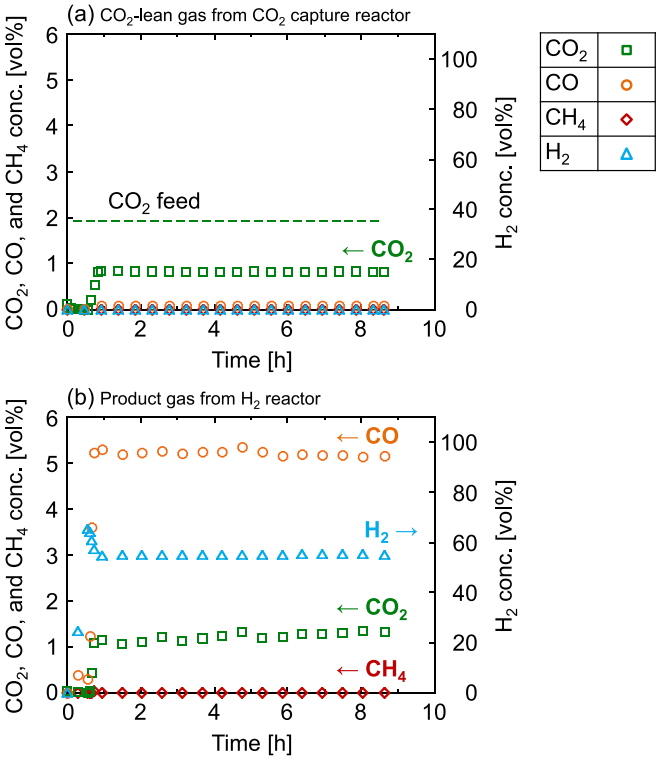

Fig. 2. Concentration profiles of (a) CO_2-lean gas exhausted from the CO_2 capture reactor at 400 °C and 8 L/min flow of 2 vol% CO_2/N_2 and (b) product gas exhausted from the H_2 reactor at 500 °C and 0.8 L/min flow of 100 % H_2.

are considered to contribute to the CO_2 capture.

$$Na_2O + CO_2 \rightleftharpoons Na_2CO_3 \quad (6)$$

$$2NaOH + CO_2 \rightleftharpoons Na_2CO_3 + H_2O \quad (7)$$

$$NaOH + CO_2 \rightleftharpoons NaHCO_3 \quad (8)$$

In addition, H_2 was not detected in the CO_2 capture reactor despite the continuous H_2 supply to the H_2 reactor, indicating that the loop seals successfully prevented the undesired mixing of gases between the two reactors.

Fig. 2(b) shows the concentration profile of the product gas exiting the H_2 reactor. The CO concentration plateaued above 5 vol% and was maintained for approximately 8 h. The captured CO_2 in the DFM was reduced to CO via the following RWGS-like reactions.

$$Na_2CO_3 + H_2 \rightleftharpoons Na_2O + CO + H_2O \quad (9)$$

$$Na_2CO_3 + H_2 \rightleftharpoons 2NaOH + CO \quad (10)$$

$$NaHCO_3 + H_2 \rightleftharpoons NaOH + CO + H_2O \quad (11)$$

The formation of CH_4 was almost negligible, and the captured CO_2 was selectively reduced to CO. However, more than 1 vol% of CO_2 was detected, indicating that a fraction of the captured CO_2 was released from the DFM without being converted into CO. The molar ratio of unreacted H_2 to the produced CO is an important factor in the direct utilization of the product gas as syngas. Although the practically feasible H_2/CO ratio for Fischer–Tropsch or methanol syntheses is 2–3, the steady-state value was approximately 11 in the present study. The inclusion of CO_2 in CO + H_2 syngas can be beneficial, as considered in industrial syngas-to-methanol processes. However, for brevity and better process controllability, the discussion in this section focuses on the H_2/CO ratio without CO_2. Methods to improve the H_2/CO ratio are discussed in Section 3.4.

The outputs from both reactors were stable over 8 h, and CCR was

expected to be repeated for more than 100 cycles during this operation, assuming the similar circulation rate of 320 cm^3/min (approximately 3 min for one cycle) to our previous result [36]. Herein, one cycle of circulation in the CFB system is represented by the DFM particles passing once through the CO_2 capture reactor and H_2 reactor (Refer to Table S3 for details). The textural properties and crystalline structures of the as-prepared and used DFM samples were compared (Table S1 and Fig. S1). No obvious degradation of DFM was observed during its use in the CFB system. Although a considerably longer stability test is necessary, the Na/Al_2O_3 DFM can enable steady-state operation.

3.3. Identifying bottlenecks of CCR in the CFB system

To identify possible bottlenecks of CCR to CO in the CFB system, the abovementioned experimental results are further discussed in comparison with our previous results [36] obtained for CCR to CH_4 by circulating the Na/Ni/Al_2O_3 DFM in an identical setup. The previous results for similar experimental conditions are shown in Fig. S3. Based on the concentration profiles of the two DFMs, the CO_2 capture efficiency (η_{CO_2}) in the CO_2 capture reactor and the CO_2 conversion (X_{CO_2}), selectivity to CO or CH_4 (S_{CO}, S_{CH_4}), and H_2 conversion (X_{H_2}) were calculated and compared (Table 1). The Na/Ni/Al_2O_3 DFM captured more than 85 % of CO_2 from the feed stream (2 vol% CO_2/N_2) in the CO_2 capture reactor, whereas the Na/Al_2O_3 DFM captured only 56 %. However, in previously reported experiments using a typical fixed-bed reactor setup, the Na/Al_2O_3 DFM exhibited a comparable CO_2 capture performance to that of the Na/Ni/Al_2O_3 DFM [20,26]. The reason for this difference is clarified through a further discussion of the H_2 reactor.

In the H_2 reactor, the Na/Al_2O_3 DFMs exhibited an excellent CO selectivity of >99 %, and the formation of CH_4 was negligible. CO_2 conversion was greater than 80 % in the absence of transition metals. The detailed reaction mechanism of the transition-metal-free DFM is currently under investigation and will be reported in the near future. Nevertheless, the CO_2 conversion using Na/Al_2O_3 was lower than that using Na/Ni/Al_2O_3, indicating that additional CO_2 was released from the DFM without being converted into products. The H_2 conversion using Na/Al_2O_3 was only one-tenth of that using Na/Ni/Al_2O_3. Although the nature of the reaction is different (RWGS vs. methanation) and the required H_2 amount differs depending on the amount of captured CO_2, the results indicate that the reaction rate of Na/Al_2O_3 in CO_2 reduction should be lower than that of Na/Ni/Al_2O_3.

In summary, the low reaction rate of Na/Al_2O_3 in CO_2 reduction is considered a bottleneck that limits the overall reaction efficiency of the CFB system. Only a fraction of the captured CO_2 is reduced to form CO in the H_2 reactor, implying that Na/Al_2O_3 is not sufficiently regenerated for the subsequent CO_2 capture. Therefore, the Na/Al_2O_3 particles, which retain CO_2, flow back into the CO_2 reactor, resulting in less CO_2 capture. Nevertheless, because the reaction behaviors in the two fluidized-bed reactors affect each other, this bottleneck should be carefully examined by changing the experimental conditions in both reactors.

Table 1
Comparison of CO_2 capture efficiency (η_{CO_2}), CO_2 conversion (X_{CO_2}), selectivity to CO or CH_4 (S_{CO}, S_{CH_4}), and H_2 conversion (X_{H_2}) with the two DFMs.

DFM	CO_2 capture reactor	H_2 reactor			
	η_{CO_2} [%]	X_{CO_2} [%]	S_{CO} [%]	S_{CH_4} [%]	X_{H_2} [%]
Na/Al_2O_3	55.7 ± 2.3	82.0 ± 4.9	99.6 ± 0.5	0.4 ± 0.5	8.1 ± 0.6
Na/Ni/Al_2O_3 [36]	>85	>99	<1	>99	>85

3.4. Effect of operating conditions in the H_2 reactor on overall CCR behavior

To overcome the bottleneck and enhance the CCR performance, the effect of the operating conditions in the H_2 reactor on the overall reaction behavior was investigated. Fig. 3 presents the experimental results for different H_2 flow rates and temperatures in the H_2 reactor. The flow rates relative to the minimum fluidization velocity at 500 °C (u/u_{mf}) are shown in the legend. The temperatures shown in the figure represent the values measured in the experiments.

Initially, the effects of the H_2 flow rate were evaluated. Fig. 3(a) shows the increase in the CO_2 capture efficiency with the H_2 flow rate, despite no change in the operating conditions of the CO_2 capture reactor. This suggests that the bottleneck in the H_2 reactor was mitigated by increasing the H_2 flow rate. The increase in the CO_2 capture efficiency was drastic when changing the H_2 flow rate from 0.4 to 0.8 L/min and was stabilized above 0.8 L/min. Similarly, the CO_2 conversion in the H_2 reactor improved when the H_2 flow rate was increased from 0.4 to 0.8 L/min, particularly at lower temperatures, whereas no significant difference was observed between 0.8 and 1.6 L/min (Fig. 3(b)). The increase in CO_2 conversion indicates a decrease in the proportion of unreacted CO_2 in the product gas in the H_2 reactor.

The marked change in performance upon increasing the H_2 flow from 0.4 to 0.8 L/min can be understood in terms of the minimum fluidization velocity, which coincides with this flow rate range (Section 3.1). Particularly, the fixed DFM bed changes to a fluidized bed in this range, resulting in a more efficient interaction and reaction between the flowing H_2 gas and DFM particles retaining CO_2. Consequently, the DFM particles are regenerated by releasing or reacting with the captured CO_2 at an H_2 flow rate of 0.8 L/min. The more effectively regenerated DFM particles return to the CO_2 capture reactor and can capture more CO_2. As shown in Fig. 3(c), particularly above the minimum fluidization velocity, the H_2 conversion at 1.6 L/min was lower than that at 0.8 L/min, indicating that the excess H_2 supply flowed out unreacted. As observed in Fig. 3(d), the H_2/CO ratio at 1.6 L/min was higher than that at 0.8 L/min. The excess H_2 resulted in higher concentrations of the unreacted H_2 and lower concentrations of the produced CO in the product gas. This is the reason for higher H_2/CO ratios with higher H_2 flow rates. On the other hand, the CO selectivity approached 99 % and was unaffected in the investigated H_2 flow rate range.

Subsequently, the effects of reaction temperature in the H_2 reactor were examined. Fig. 3(a)–(c) show that the CO_2 capture efficiency, CO_2 conversion, and H_2 conversion increase with increasing temperature. Higher hydrogenation temperatures favor endothermic CO formation reactions (Eqs. (9)–(11)) in terms of both thermodynamics and kinetics; therefore, these interrelated characteristics improved with increasing temperature. Particularly, the H_2/CO ratio decreased with increasing temperature and approached 6 at 0.8 L/min and the highest temperature in the H_2 reactor. Although the H_2/CO ratio was still as high as that of practical syngas, this experimental result confirmed that the H_2/CO ratio could be controlled depending on the operating conditions. However, the CO selectivity was not affected by the temperature in the H_2 reactor or the H_2 flow rate in the studied range.

Therefore, the CFB system shows better CCR performance at H_2 flow rates that are slightly higher than the minimum fluidization velocity and at higher temperatures. Nonetheless, the originally white DFM particles gradually turned gray as the temperature increased above 600 °C (data not shown). This could be attributed to the deposition of carbon by coking reactions, which may decrease the activity of the DFM. Further investigation is necessary to determine the optimum temperature for balancing the reaction efficiency and durability of the DFM.

3.5. Effect of operating conditions in the CO_2 reactor on overall behavior

Furthermore, the effects of the operating conditions of the CO_2 capture reactor on the overall reaction behavior were investigated.

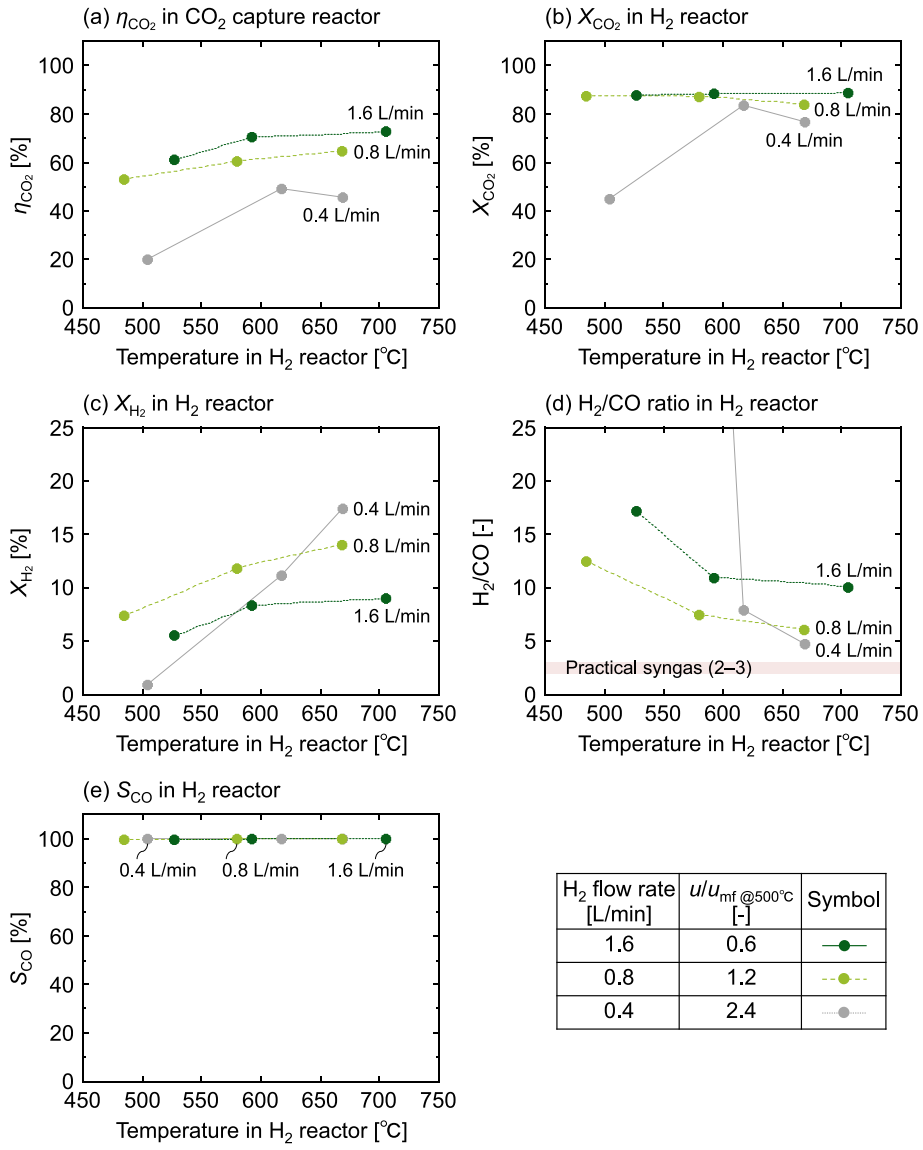

H_2 flow rate [L/min]	$u/u_{mf\,@500°C}$ [-]	Symbol
1.6	0.6	
0.8	1.2	
0.4	2.4	

Fig. 3. Effect of H_2 flow rate and temperature in the H_2 reactor on (a) CO_2 capture efficiency in the CO_2 capture reactor and on (b) CO_2 and (c) H_2 conversion, (d) H_2/CO ratio, and (e) selectivity of CO in the H_2 reactor.

Because the feed flow rate to the CO_2 capture reactor is a critical engineering factor that can disrupt the smooth circulation of DFM particles, only the effect of temperature was studied. Fig. 4 depicts the experimental results wherein the H_2 flow rate and temperature in the H_2 reactor were set to 0.8 L/min and 500 °C, respectively, based on the abovementioned discussion. The CO_2 capture efficiency slightly increased upon decreasing the temperature in the CO_2 capture reactor, because exothermic CO_2 capture reactions (Eqs. (6)–(8)) thermodynamically favor lower temperatures.

As the CO_2 capture efficiency increased, additional CO_2 was introduced into the H_2 reactor by the DFM particles, thereby increasing the H_2 conversion. Consequently, the H_2/CO ratio was decreased. The CO_2 conversion in the H_2 reactor decreased slightly with increasing temperature in the CO_2 capture reactor, whereas the CO selectivity remained constant. This trend suggests that a greater inflow of CO_2 (as captured in the DFM) into the H_2 reactor increased the proportion of desorbed CO_2 that was not reduced to CO. To suppress the decrease in CO_2 conversion, the reaction efficiency must be improved in terms of kinetics by catalyst engineering in the H_2 reactor (Section 3.3).

4. Conclusion

Transition metal-free Na/Al_2O_3 DFM particles were circulated between two fluidized-bed reactors for CCR. In the CO_2 capture reactor, approximately half of the supplied CO_2 was continuously captured by the DFM. Subsequently, the CO_2 captured in the DFM was reduced in the H_2 reactor and a syngas-like mixture of H_2/CO was obtained; the CO_2 conversion and CO selectivity exceeded 80 % and 99 %, respectively. The effluent gas concentrations from both reactors were stable for more than 8 h, indicating the successful demonstration of continuous and steady-state CCR of syngas using the Na/Al_2O_3 DFM in the CFB system. However, the H_2 conversion was less than 20 % under the studied conditions, and H_2/CO was still exceedingly high for the direct use of the product gas as syngas. If the H_2 conversion is successfully improved to produce additional CO, the H_2/CO ratio can fall within the target range. This study confirms that the H_2/CO ratio can be controlled by varying the reaction conditions, such as the H_2 flow rate. Although longer residence time of the feed gas would be beneficial to compensate for the slow reaction kinetics of the transition-metal-free DFM, the gas flow rate should excess the minimum fluidization velocity in the CFB system. Accordingly, the dimensions and configuration of the CFB system will be

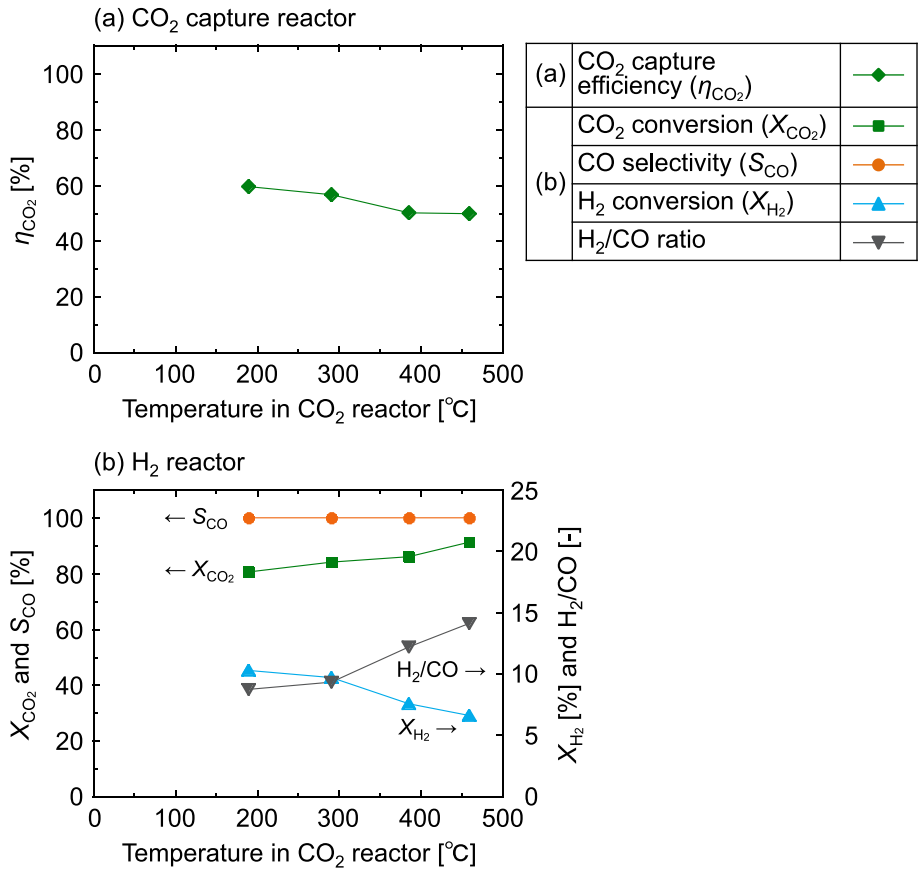

Fig. 4. Effect of temperature in the CO_2 capture reactor on (a) CO_2 capture efficiency in the CO_2 capture reactor and on (b) conversions of CO_2 and H_2, selectivity of CO, and H_2/CO ratio in the H_2 reactor.

effectively upgraded in the near future to enhance the interaction between the reaction gas and DFM particles.

CRediT authorship contribution statement

Tomone Sasayama: Writing – original draft, Visualization, Methodology, Investigation, Formal analysis. **Yuya Ono:** Methodology, Investigation. **Fumihiko Kosaka:** Writing – review & editing, Methodology, Investigation. **Yanyong Liu:** Conceptualization. **Shih-Yuan Chen:** Writing – review & editing. **Takehisa Mochizuki:** Conceptualization. **Koichi Matsuoka:** Writing – review & editing, Supervision, Methodology. **Atsushi Urakawa:** Writing – review & editing, Validation, Supervision. **Koji Kuramoto:** Writing – review & editing, Project administration, Methodology.

Declaration of competing interest

The authors declare that they have no known competing financial interests or personal relationships that could have appeared to influence the work reported in this paper.

Data availability

Data will be made available on request.

Acknowledgements

This research did not receive any specific grant from funding agencies in the public, commercial, or not-for-profit sectors.

Appendix A. Supplementary data

Supplementary data to this article can be found online at https://doi.org/10.1016/j.seppur.2024.128602.

References

[1] IPCC6th Working Group 1 Report, 2021.
[2] IPCC6th Working Group 3Report, 2022.
[3] M.A. Sabri, S. Al Jitan, D. Bahamon, L.F. Vega, G. Palmisano, Current and future perspectives on catalytic-based integrated carbon capture and utilization, Sci. Total Environ. 790 (2021) 148081, https://doi.org/10.1016/j.scitotenv.2021.148081.
[4] L. Zhang, Y. Song, J. Shi, Q. Shen, D. Hu, Q. Gao, W. Chen, K.-W. Kow, C. Pang, N. Sun, W. Wei, Frontiers of CO_2 Capture and Utilization (CCU) towards carbon neutrality, Adv. Atmos. Sci. 39 (2022) 1252–1270, https://doi.org/10.1007/s00376-022-1467-x.
[5] K. Zhang, D. Guo, X. Wang, Y. Qin, L. Hu, Y. Zhang, R. Zou, S. Gao, Sustainable CO_2 management through integrated CO_2 capture and conversion, J. CO_2 Util. 72 (2023) 102493, https://doi.org/10.1016/j.jcou.2023.102493.
[6] Y. Zhang, S. Zhao, L. Li, J. Feng, K. Li, Z. Huang, H. Lin, Integrated CO_2 capture and utilization: a review of the synergistic effects of dual function materials, Catal. Sci. Technol. 14 (2024) 790–819, https://doi.org/10.1039/D3CY01289A.
[7] B. Jin, R. Wang, D. Fu, T. Ouyang, Y. Fan, H. Zhang, Z. Liang, Chemical looping CO_2 capture and in-situ conversion as a promising platform for green and low-carbon industry transition: review and perspective, Carbon Capt. Sci. Technol. 10 (2024) 100169, https://doi.org/10.1016/j.ccst.2023.100169.
[8] B. Jin, K. Wei, T. Ouyang, Y. Fan, H. Zhao, H. Zhang, Z. Liang, Chemical looping CO_2 capture and in-situ conversion: fundamentals, process configurations, bifunctional materials, and reaction mechanisms, Appl. Energy Combust. Sci. 16 (2023) 100218, https://doi.org/10.1016/j.jaecs.2023.100218.
[9] C. Reller, M. Pöge, A. Lißner, F.O.R.L. Mertens, Methanol from CO_2 by organo-cocatalysis: CO_2 capture and hydrogenation in one process step, Environ. Sci. Technol. 48 (2014) 14799–14804, https://doi.org/10.1021/es503914d.
[10] N.M. Rezayee, C.A. Huff, M.S. Sanford, Tandem amine and ruthenium-catalyzed hydrogenation of CO_2 to methanol, J. Am. Chem. Soc. 137 (2015) 1028–1031, https://doi.org/10.1021/ja511329m.
[11] S. Kar, R. Sen, A. Goeppert, G.K.S. Prakash, Integrative CO_2 capture and hydrogenation to methanol with reusable catalyst and amine: toward a carbon

neutral methanol economy, J. Am. Chem. Soc. 140 (2018) 1580–1583, https://doi.org/10.1021/jacs.7b12183.
[12] L.A. Diaz, N. Gao, B. Adhikari, T.E. Lister, E.J. Dufek, A.D. Wilson, Electrochemical production of syngas from CO_2 captured in switchable polarity solvents, Green Chem. 20 (2018) 620–626, https://doi.org/10.1039/C7GC03069J.
[13] E. Pérez-Gallent, C. Vankani, C. Sánchez-Martínez, A. Anastasopol, E. Goetheer, Integrating CO_2 capture with electrochemical conversion using amine-based capture solvents as electrolytes, Ind. Eng. Chem. Res. 60 (2021) 4269–4278, https://doi.org/10.1021/acs.iecr.0c05848.
[14] C. Gouedard, D. Picq, F. Launay, P.-L. Carrette, Amine degradation in CO_2 capture. I. A review, Int. J. Greenhouse Gas Control 10 (2012) 244–270, https://doi.org/10.1016/j.ijggc.2012.06.015.
[15] B.R. Strazisar, R.R. Anderson, C.M. White, Degradation pathways for monoethanolamine in a CO_2 capture facility, Energy Fuels 17 (2003) 1034–1039, https://doi.org/10.1021/ef020272i.
[16] J. Davis, G. Rochelle, Thermal degradation of monoethanolamine at stripper conditions, Energy Proc. 1 (2009) 327–333, https://doi.org/10.1016/j.egypro.2009.01.045.
[17] M.S. Duyar, M.A.A. Treviño, R.J. Farrauto, Dual function materials for CO_2 capture and conversion using renewable H_2, Appl. Catal. B 168–169 (2015) 370–376, https://doi.org/10.1016/j.apcatb.2014.12.025.
[18] L.F. Bobadilla, J.M. Riesco-García, G. Penelás-Pérez, A. Urakawa, Enabling continuous capture and catalytic conversion of flue gas CO_2 to syngas in one process, J. CO_2 Util. 14 (2016) 106–111, https://doi.org/10.1016/j.jcou.2016.04.003.
[19] C. Jeong-Potter, A. Zangiabadi, R. Farrauto, Extended aging of Ru-Ni, Na_2O/Al_2O_3 dual function materials (DFM) for combined capture and subsequent catalytic methanation of CO_2 from power plant flue gas, Fuel 328 (2022) 125283, https://doi.org/10.1016/j.fuel.2022.125283.
[20] T. Sasayama, F. Kosaka, Y. Liu, T. Yamaguchi, S.-Y. Chen, T. Mochizuki, A. Urakawa, K. Kuramoto, Integrated CO_2 capture and selective conversion to syngas using transition-metal-free Na/Al_2O_3 dual-function material, J. CO_2 Util. 60 (2022) 102049, https://doi.org/10.1016/j.jcou.2022.102049.
[21] T. Hyakutake, W. van Beek, A. Urakawa, Unravelling the nature, evolution and spatial gradients of active species and active sites in the catalyst bed of unpromoted and K/Ba-promoted Cu/Al2O3 during CO_2 capture-reduction, J. Mater. Chem. A 4 (2016) 6878–6885, https://doi.org/10.1039/C5TA09461E.
[22] D. Pinto, V. van der B. Estadella, A. Urakawa, Mechanistic insights into the CO_2 capture and reduction on K-promoted Cu/Al_2O_3 by spatiotemporal operando methodologies, Catal. Sci. Technol. 12 (2022) 5349–5359, https://doi.org/10.1039/D2CY00228K.
[23] H. Sun, J. Wang, J. Zhao, B. Shen, J. Shi, J. Huang, C. Wu, Dual functional catalytic materials of Ni over Ce-modified CaO sorbents for integrated CO_2 capture and conversion, Appl. Catal. B 244 (2019) 63–75, https://doi.org/10.1016/j.apcatb.2018.11.040.
[24] J. Hu, P. Hongmanorom, V.V. Galvita, Z. Li, S. Kawi, Bifunctional Ni-Ca based material for integrated CO_2 capture and conversion via calcium-looping dry reforming, Appl. Catal. B 284 (2021) 119734, https://doi.org/10.1016/j.apcatb.2020.119734.
[25] S. Sun, H. Sun, P.T. Williams, C. Wu, Recent advances in integrated CO_2 capture and utilization: a review, Sust. Energy Fuels 5 (2021) 4546–4559, https://doi.org/10.1039/D1SE00797A.
[26] F. Kosaka, Y. Liu, S.-Y. Chen, T. Mochizuki, H. Takagi, A. Urakawa, K. Kuramoto, Enhanced activity of integrated CO_2 capture and reduction to CH_4 under pressurized conditions toward atmospheric CO_2 utilization, ACS Sust. Chem. Eng. 9 (2021) 3452–3463, https://doi.org/10.1021/acssuschemeng.0c07162.
[27] J. Lee, J. Otomo, Proton conduction-assisted direct CO_2 methanation using Ni/CaO/Y-doped $BaZrO_3$ proton conductor, Fuel 322 (2022) 124094, https://doi.org/10.1016/j.fuel.2022.124094.
[28] Y. Guo, G. Wang, J. Yu, P. Huang, J. Sun, R. Wang, T. Wang, C. Zhao, Tailoring the performance of Ni-CaO dual function materials for integrated CO_2 capture and conversion by doping transition metal oxides, Separ. Purif. Technol. 305 (2023) 122455, https://doi.org/10.1016/j.seppur.2022.122455.
[29] R. Han, S. Xing, Y. Wang, L. Wei, Z. Li, C. Yang, C. Song, Q. Liu, Two birds with one stone: MgO promoted Ni-CaO as stable and coke-resistant bifunctional materials for integrated CO_2 capture and conversion, Sep. Purif. Technol. 307 (2023) 122808, https://doi.org/10.1016/j.seppur.2022.122808.
[30] A. Bermejo-López, B. Pereda-Ayo, J.A. Onrubia-Calvo, J.A. González-Marcos, J. R. González-Velasco, Tuning basicity of dual function materials widens operation temperature window for efficient CO_2 adsorption and hydrogenation to CH_4, J. CO_2 Util. 58 (2022) 101922, https://doi.org/10.1016/j.jcou.2022.101922.
[31] C. Jeong-Potter, M. Abdallah, C. Sanderson, M. Goldman, R. Gupta, R. Farrauto, Dual function materials ($Ru+Na_2O/Al_2O_3$) for direct air capture of CO_2 and in situ catalytic methanation: the impact of realistic ambient conditions, Appl. Catal. B 307 (2022) 120990, https://doi.org/10.1016/j.apcatb.2021.120990.
[32] S.B. Jo, J.H. Woo, J.H. Lee, T.Y. Kim, H.I. Kang, S.C. Lee, J.C. Kim, CO_2 green technologies in CO_2 capture and direct utilization processes: methanation, reverse water-gas shift, and dry reforming of methane, Sust. Energy Fuels 4 (2020) 5543–5549, https://doi.org/10.1039/D0SE00951B.
[33] L.-P. Merkouri, T.R. Reina, M.S. Duyar, Feasibility of switchable dual function materials as a flexible technology for CO_2 capture and utilisation and evidence of passive direct air capture, Nanoscale (2022), https://doi.org/10.1039/D2NR02688K.
[34] L. Li, Z. Wu, S. Miyazaki, T. Toyao, Z. Maeno, K. Shimizu, Continuous CO_2 capture and methanation over $Ni–Ca/Al_2O_3$ dual functional materials, RSC Adv. 13 (2023) 2213–2219, https://doi.org/10.1039/D2RA07554G.
[35] L. Li, S. Miyazaki, S. Yasumura, K.W. Ting, T. Toyao, Z. Maeno, K. Shimizu, Continuous CO_2 capture and selective hydrogenation to CO over Na-promoted Pt nanoparticles on Al_2O_3, ACS Catal. 12 (2022) 2639–2650, https://doi.org/10.1021/acscatal.1c05339.
[36] F. Kosaka, T. Sasayama, Y. Liu, S.-Y. Chen, T. Mochizuki, K. Matsuoka, A. Urakawa, K. Kuramoto, Direct and continuous conversion of flue gas CO_2 into green fuels using dual function materials in a circulating fluidized bed system, Chem. Eng. J. 450 (2022) 138055, https://doi.org/10.1016/j.cej.2022.138055.